Annals of the Academy of Romanian Scientists
Series on Science and Technology of Information
ISSN 2066-8562 Volume **3**, Number **1**/**2010**

NUMERICAL SIMULATION USING PARTIAL DIFFERENTIAL EQUATIONS FOR MODELING AND CONTROL OF MEDICAL RADIATION FIELDS

Nicolae Marius ROMAN[1],
Horaţiu Alexandru COLOŞI[2], Mircea Valer PUŞCĂ[3]

Rezumat. *Această lucrare prezintă o nouă abordare, bazată pe un model de ecuaţii cu derivate parţiale (EDP), pentru modelarea analogică şi simularea numerică a proceselor biomedicale cu parametrii distribuiţi. Astfel de procese redau penetrarea radiaţiilor în radioterapie sau în tehnicile de investigare radiologică. Studiul de faţă simulează propagarea prin diferite medii. O caracteristică importantă a metodei propuse este aceea de a simula propagarea prin medii neomogene, cum ar fi ţesuturile umane. Lucrarea oferă un punct de plecare în tehnica controlului automat al dispozitivelor radiologice.*

Abstract. *This paper presents a novel approach, based on a partial differential equation (PDE) model, for analogical modeling and digital simulation of biomedical processes with distributed parameters. Such processes include penetration of radiation during radiation therapy or radiological imaging techniques. The present study simulates the propagation of radiation through different media. A valuable feature of the proposed method is its ability to simulate propagation along inhomogeneous media such as human tissues. It offers a starting point for automated control of radiological devices.*

Keywords: partial differential equations, distributed parameters, radiation field, propagation

1. Introduction

Medical research and practice offers numerous applications for numerical simulation [1-4]. One such application, automated control of radiation field intensity generated during radiation therapy, constitutes an efficient method to reduce unnecessary radiation exposure for both patient and device operator [5, 6]. The aim of our study has been to develop a model for radiation field control at various tissue locations investigated or treated using radiological devices.

The phenomenon of radiological field spreading is represented on Cartesian coordinate system (0p; 0q; 0r) in figure 1. A possible pattern of spread is considered, particularly in relation to these axes and in relation to time (*t*). The radiation field intensity *y(t, p, q, r)* is shown in figures 1b, 1c, and 1d, in which:

[1]Prof., Ph.D., Electrical Engineering Faculty, Technical University of Cluj-Napoca, Cluj-Napoca, Romania (Marius.Roman@et.utcluj.ro).
[2]Assist. Prof., Ph.D., University of Medicine and Pharmacy "Iuliu Haţieganu", Cluj-Napoca, Romania (hcolosi@umfcluj.ro).
[3]Senior Researcher, Electrical Engineering Faculty, Technical University of Cluj Napoca, Cluj Napoca, Romania (mvpusca@yahoo.com).

$$y(t, p, q, r) = y_{00}[t, s, u(t)] = K_y \cdot F_{0T}(t) \cdot F_{0S}(s) \cdot u(t). \quad (1)$$

The following variables and function were considered in a Cartesian space:

$$s = \pm\sqrt{p^2 + q^2 + r^2}; \quad s_f = \pm\sqrt{{p_f}^2 + {q_f}^2 + {r_f}^2} \quad (2)$$

$$F_{0S}(s) = \pm\sqrt{{F_{0P}}^2(p) + {F_{0Q}}^2(q) + {F_{0R}}^2(r)}, \quad (3)$$

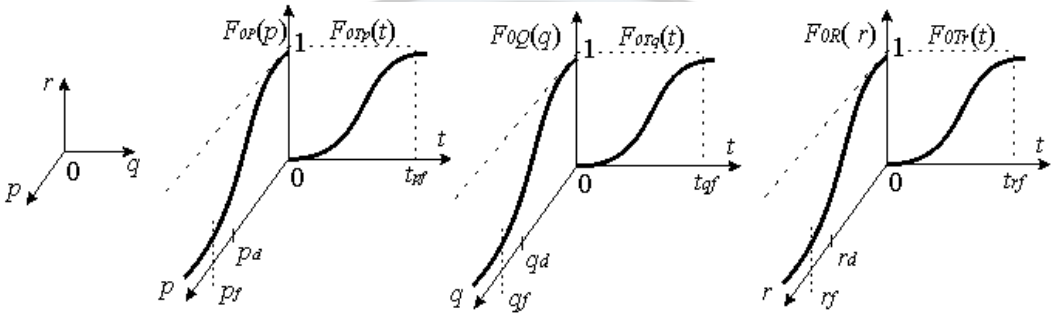

Fig. 1. Representation of radiation field intensity, *y(t, p, q, r)* in Cartesian coordinate system:
a. Cartesian system **b.** *y* on 0*p* axis **c.** *y* on 0*q* axis; **d.** *y* on 0*r* axis.

where:

$$F_{0P}(p) = \frac{P_1}{P_1 - P_2}\varepsilon^{-\frac{\text{abs}(p)}{P_1}} + \frac{P_2}{P_2 - P_1}\cdot\varepsilon^{-\frac{\text{abs}(p)}{P_2}} \quad (4)$$

$$F_{0Q}(q) = \frac{Q_1}{Q_1 - Q_2}\varepsilon^{-\frac{\text{abs}(q)}{Q_1}} + \frac{Q_2}{Q_2 - Q_1}\cdot\varepsilon^{-\frac{\text{abs}(q)}{Q_2}} \quad (5)$$

$$F_{0R}(r) = \frac{R_1}{R_1 - R_2}\varepsilon^{-\frac{\text{abs}(r)}{R_1}} + \frac{R_2}{R_2 - R_1}\cdot\varepsilon^{-\frac{\text{abs}(r)}{R_2}} \quad (6)$$

The axes (0*p*) and (0*q*) define the horizontal plane, in which the field generator is located. Field intensity expressed in (1), and axis (0*r*) correspond to the depth of field propagation. The constants in (4), (5), (6) can be approximated by expert procedures, namely:

$$P_1 = \frac{p_f}{\mu_P(1+\lambda_P)} \; ; \quad P_2 = \lambda_P \cdot P_1, \quad \text{where: } \mu_P = (4 \div 6) \text{ and } \lambda_P > 1 \quad (7)$$

$$Q_1 = \frac{q_f}{\mu_Q(1+\lambda_Q)} \; ; \quad Q_2 = \lambda_Q \cdot Q_1, \quad \text{where: } \mu_Q = (4 \div 6) \text{ and } \lambda_Q > 1 \quad (8)$$

$$R_1 = \frac{r_f}{\mu_R(1+\lambda_R)} \; ; \quad R_2 = \lambda_R \cdot R_1, \quad \text{where: } \mu_R = (4 \div 6) \text{ and } \lambda_R > 1 \quad (9)$$

where the final abscises $(p_f), (q_f), (r_f)$ correspond to negligible values (for example ≤ 0.05).

For $F_{0P}(p)$, $F_{0Q}(q), F_{0R}(r)$, the abscises $(p_d), (q_d), (r_d)$ may show perturbations (discontinuities in tissue structure), estimated by:

$$F_{0S}(s) = \frac{S_1}{S_1 - S_2}\varepsilon^{-\frac{abs(s)}{S_1}} + \frac{S_2}{S_2 - S_1}\cdot\varepsilon^{-\frac{abs(s)}{S_2}}, \text{ where:} \tag{10}$$

$$S_1 = \frac{s_f}{\mu_S \cdot (1+\lambda_S)}\ ; \quad S_2 = \lambda_S \cdot S_1 \tag{11}$$

$$\mu_S = \frac{p_f + q_f + r_f}{\frac{p_f}{\mu_P} + \frac{q_f}{\mu_Q} + \frac{r_f}{\mu_R}}; \quad \lambda_S = \frac{P_2 + Q_2 + R_2}{P_1 + Q_1 + R_1}. \tag{12}$$

Therefore, $F_{0S}(s)$ can also be written:

$$F_{0S}(s) = \frac{1}{1-\lambda_S}\cdot\left[\varepsilon^{-\frac{\mu_S(1+\lambda_S)}{s_f}\cdot abs(s)} - \lambda_S \cdot \varepsilon^{-\frac{\mu_S(1+\lambda_S)}{s_f}\cdot abs(s)}\right] \tag{13}$$

or:
$$F_{0S}(s) = C_0 \cdot \left(\varepsilon^{C_1\cdot\sqrt{p^2+q^2+r^2}} + C_2 \cdot \varepsilon^{C_3\sqrt{p^2+q^2+r^2}}\right) \tag{14}$$

where:
$$C_0 = \frac{1}{1-\lambda_S}\ ; \quad C_1 = \frac{\mu_S(1+\lambda_S)}{s_f}; \quad C_2 = -\lambda_S\ ; \quad C_3 = \frac{1}{\lambda_S}\cdot C_1 \tag{15}$$

The results of $F_{0S}(s)$ from (4), (10), (13) and (14) also represent spatial curves deformed by multiple degrees of freedom, for example $(\mu_S), (\lambda_S)$ and (s_f), while the "length constants" $(P\ldots)$, $(Q\ldots)$ and $(R\ldots)$ may exhibit "inertia" or "attenuation" of radiological propagation in a tissue.

Function components $F_{0P}(p), F_{0Q}(q)$ or $F_{0R}(r)$ can be approximated by:

$$F_{0vd}(v) = A_{vd}\cdot\varepsilon^{-K_{vd}(v_d - v)^2} \tag{16}$$

in which the variable (v) can be (p), (q) or (r), by case.

The disturbance index (*d*) refers to the homogeneity disturbance due to tissue heterogeneity located on the abscissa (v_d), while (A_{vd}) in (16) represents the amplitude of heterogeneity illustrated in figure 2.a.

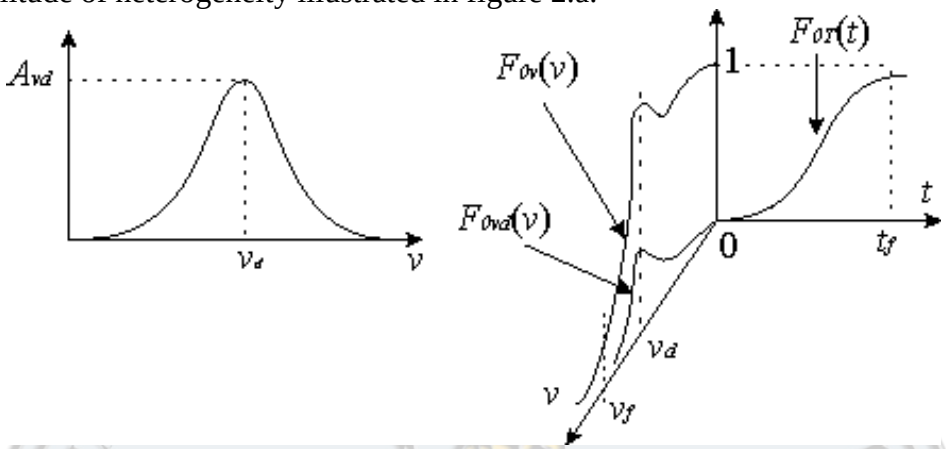

Fig. 2. Tissue heterogeneity may lead to homogeneity disturbances of field intensity: **a.** Amplitude **b.** Trajectory in Cartesian space.

By convenient choice of the parameter (K_{vd}) a more or less steep (and symmetrical) slope can be ensured. In figure 5b, the deformation effect of function $F_{0vd}(v)$ on the right abscissa (v_d) over the component $F_{0v}(v)$ can be seen. If, with respect to time, the spread of radiological field intensity $y(t,p,q,r)$ was identical on all three axes (0*p*), (0*q*) and (0*r*) in figures 1b, 1c and 1d, then:

$$F_{0Tp}(t) = F_{0Tq}(t) = F_{0Tr}(t) = F_{0T}(t) \tag{17}$$

which may also be approximated as a customary form of step response, in relation to the control signal $u(t)$ applied to the radiological source. Thus:

$$F_{0T}(t) = 1 - \frac{T_1}{T_1 - T_2}\varepsilon^{-\frac{t}{T_1}} - \frac{T_2}{T_2 - T_1}\varepsilon^{-\frac{t}{T_2}} \tag{18}$$

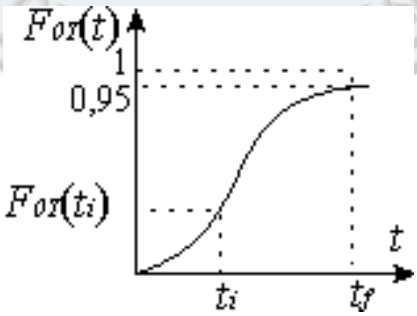

Fig. 3. Transient phenomenon.

The length (t_f) of this transient phenomenon (figure 3) reflects a radiation propagation inertia, identical on axes (*p, q, r, s*) for which $t > t_f$ tends to the unitary asymptote.

For this slow or fast ascending evolution we considered $\mu_T \cong 4 \div 6,\ \lambda_T > 1$, resulting in the following time constants:

$$T_1 = \frac{t_f}{\mu_\tau \cdot (1+\lambda_\tau)};\quad T_2 = \lambda_\tau \cdot T_1;\quad t_i = \frac{T_1 \cdot T_2}{T_2 - T_1} \cdot \ln\left(\frac{T_2}{T_1}\right) \tag{19}$$

where (t_i) is the moment corresponding to the inflexion $F_{0\tau}(t_i)$.

It can be seen in figures 1b, 1c, 1d, and 2 that the final values (p_f, q_f, r_f, v_f) show the depth of the radiological penetration which depends on the control signal and on the more or less homogeneous structure of the environment (tissue).

If this spread inertia is different in relation to the axes, then condition (17) is not accomplished, resulting in:

$$F_{0Tp}(t) \neq F_{0Tq}(t) \neq F_{0Tr}(t) \tag{20}$$

In this case, formally identical to relation (19), each axis will exhibit:

$$T_{1p} = \frac{t_{pf}}{\mu_{Tq} \cdot (1+\lambda_{Tp})};\quad T_{2p} = \lambda_{Tp} \cdot T_{1p} \tag{21}$$

$$T_{1q} = \frac{t_{qf}}{\mu_{Tq} \cdot (1+\lambda_{Tq})};\quad T_{2q} = \lambda_{Tq} T_{1q} \tag{22}$$

$$T_{1r} = \frac{t_{rf}}{\mu_{Tr} \cdot (1+\lambda_{Tr})};\quad T_{2r} = \lambda_{Tr} T_{1r} \tag{23}$$

where $(t_{...f})$, $(\mu_{T...})$ and $(\lambda_{T...})$ are specifically established for each axis.

To transform into Cartesian coordinates it can be shown that:

$$\mu_\tau = \frac{t_{pf} + t_{qf} + t_{rf}}{T_{1p} + T_{2p} + T_{1q} + T_{2q} + T_{1r} + T_{2r}};\ \lambda_\tau = \frac{T_{2p} + T_{2q} + T_{2r}}{T_{1p} + T_{1q} + T_{1r}} \tag{24}$$

finally resulting in:

$$T_1 = \frac{t_f}{\mu_\tau \cdot (1+\lambda_\tau)};\quad T_2 = \lambda_\tau \cdot T_1 \tag{25}$$

which are the equivalent time constants of the Cartesian space, assuming that inertial propagations are different along the three axes (*p, q, r*).

Following this method, $F_{0T}(t)$ from (1) becomes:

$$F_{0T}(t) = \frac{T_1}{T_1 - T_2} \cdot \varepsilon^{-\frac{t}{T_1}} + \frac{T_2}{T_2 - T_1} \cdot \varepsilon^{-\frac{t}{T_2}} \tag{26}$$

which together with F_{0S} (s) from (10), allows the establishment of the radiological field intensity from figure (1),

$$y_{00}[t, s, u(t)] = K_y \cdot F_{00}(t, s) \cdot u_{S0}(t), \tag{27}$$

where $F_{00}(t, s) = F_{0T}(t) \cdot F_{0S}(s)$ and (K_y) is a weighting coefficient.

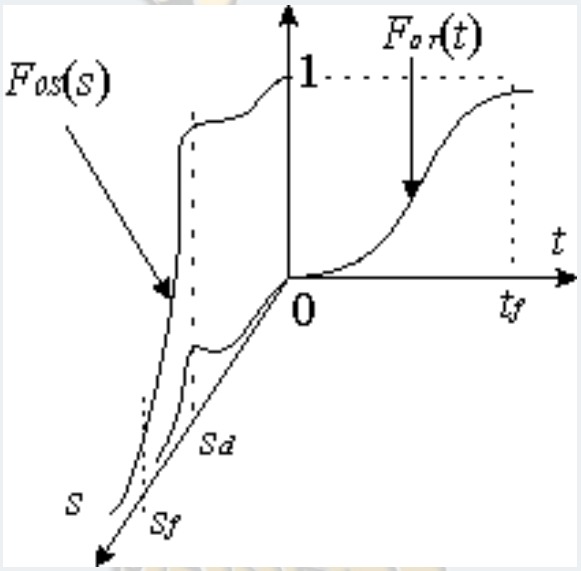

Fig. 4. F_{OT} and F_{OS} variations.

For the two functions $F_{0T}(t)$ and $F_{0S}(s)$ exemplified in Cartesian space in figure (4), the relations become obvious:

$$t_f = \sqrt{t_{pf}^2 + t_{qf}^2 + t_{rf}^2}\ ;\ \ s_f = \sqrt{p_f^2 + q_f^2 + r_f^2}\ ;\ \ s_d = \sqrt{p_d^2 + q_d^2 + r_d^2}\,, \tag{28}$$

as they were given in figures 1b, 1c, 1d and 2.

2. Analogical modeling of the proposed adjustment scheme

In figure 5 a block diagram for adjusting the radiological field with components modeled by algebraic and differential (29), (30), and partial differential equations (31) is presented.

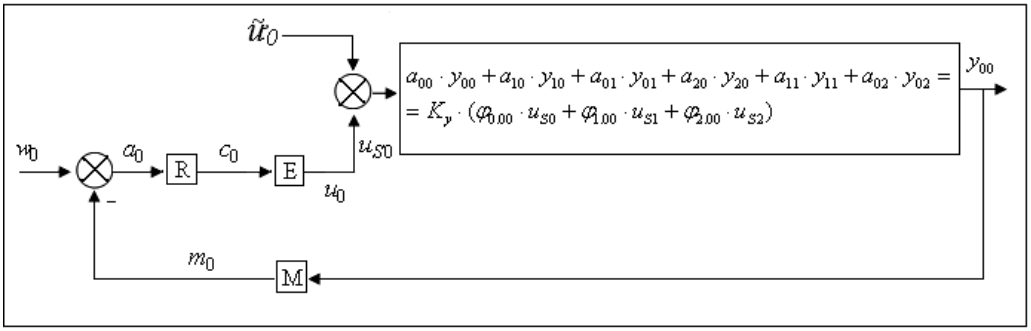

Fig. 5. Block diagram of the proposed adjustment scheme.

$$a_0 = w_0 - m_o; \quad K_m \cdot y_{00} = m_0 + T_m \cdot m_1 \tag{29}$$

$$K_{IR} \cdot a_0 + K_{PR} \cdot a_1 + K_{DR} \cdot a_2 = c_1 + T_R \cdot c_2; \quad K_E \cdot c_0 = u_0 + T_E \cdot u_1 \tag{30}$$

$$a_{00} \cdot y_{00} + a_{10} \cdot y_{10} + a_{01} \cdot y_{01} + a_{20} \cdot y_{20} + a_{11} \cdot y_{11} + a_{02} \cdot y_{02} =$$
$$= K_y \cdot (\varphi_{0.00} \cdot u_{S0} + \varphi_{1.00} \cdot u_{S1} + \varphi_{2.00} \cdot u_{S2}) \tag{31}$$

The indexes in relations (29), (30) and the first parameter from relation (31), correspond to the order of derivative with respect to time (*t*), and the second parameter from (31) corresponds to the order of derivative with respect to variable (s) defined in relation (2). Considering the example:

$$c_2 = \frac{d^2 \cdot c_0}{dt^2}, \; y_{11} = \frac{\partial^2 \cdot y_{00}}{\partial t \cdot \partial s}, \; y_{02} = \frac{d^2 \cdot y_{00}}{ds^2}, \; u_{s1} = \frac{d \cdot u_{S0}}{dt},$$

the radiological field (y_{00}) defined in (26) is converted into electrical signal (m_0) by the measurement transducer *M* from (29).

The control error (a_0) results from (29), where (w_0) is the reference signal. The *R* controller with *PID* behavior from (30) is emitting a control signal (c_0), applied to the electromagnetic field generator *E* (microwave), also defined in relation (30). The radiation emitting unit, E, generates the execution signal (u_0) representing the incident radiological field which is applied to the propagation environments (e.g. air, tissues) together with a possible resultant perturbation signal ($\tilde{u}r_0$), resulting in:

$$u_{S0} = u_0 \pm \tilde{u}r_0 \tag{32}$$

In this case ($\tilde{u}r_0$) corresponds to the homogeneity perturbation $F_{ovd}(v)$ from (16), where $v = s_d$ found in (28).

Thus, the complex phenomenon of radiological propagation is estimated by partial differential equation (31). In the left member of this equation we introduced the

approximated solution (27), resulting in the right member:

$$\phi_{0.00} = a_{00} \cdot F_{00} + a_{10} \cdot F_{10} + a_{01} \cdot F_{01} + a_{20} \cdot F_{20} + a_{11} \cdot F_{11} + a_{02} \cdot F_{02} \qquad (33)$$

$$\varphi_{01.00} = a_{10} \cdot F_{00} + 2 \cdot a_{20} \cdot F_{10} + a_{11} \cdot F_{01} \qquad (34)$$

$$\varphi_{2.00} = a_{20} \cdot F_{00} \qquad (35)$$

in which partial derivatives ($F_{0...}$), (F_{11}) and ($F_{...0}$) are obtained from relation (27). Only signal (u_0) is included in the block diagram. The disturbance ($\tilde{u}r_0$) is an independent external signal.

From the equation system (28)…(31), the matrix with partial derivatives of the state vector (M_{dpx}) represented in (36) has been deduced for the entire regulation system in figure 5. In (36), the state vector ***x*** has the following transposed form:

$$x^T = \boxed{m_0}\boxed{m_1}\boxed{c_0}\boxed{c_1}\boxed{u_0}\boxed{y_{00}}\boxed{y_{10}}$$

Because the signals $m = m(t)$, $c = c(t)$ and $u = u(t)$ are functions only of time, all their partial derivatives with respect to (s) are equal to zero. Details concerning the preparation and analogical modeling of systems through (M_{dpx}) may be found in [7, 8]. In our case, (M_{dpx}) from (36) is composed by:

$x(8\times1)$ state vector,
$x_S(8\times6)$ state vector derivative with respect to variable (s),
$x_T(20\times1)$ state vector derivative with respect to variable (t),
$x_{TS}(20\times6)$, state vector derivative with respect to variables (t) and (s).

3. Numerical simulation by $(\mathbf{M_{dpx}})$ and Taylor series

Numerical simulation requires knowledge of initial conditions CI(t_0,s), for $x_{CI} = x(t_0, s) = x_{k-1}$, from which results by partial derivative with respect to (s):

$$x_{S,CI} = x_s(t_0, s) = x_{S,k-1}$$

in which sequence $(k-1)$ corresponds to the moment $t_{k-1} = (k-1) \cdot \Delta t$, and sequence ($k$) corresponds to $t_k = k \cdot \Delta t$, where (Δt) is a sufficiently small integration step.

Using (x_{CI}) and $(x_{S,CI})$ above, we computed using specific operations based on symbolic derivatives by indices, the composing elements of (x_T) and (x_{TS}) resulting in:

$$x_{T,CI} = x_T(t_0, s) = x_{T,k-1} \text{ and } x_{TS,CI} = x_{TS}(t_0, s) = x_{TS,k-1}.$$

$$M_{dpx} = \begin{array}{|c|c|}\hline x & x_S \\ \hline x_T & x_{TS} \\ \hline \end{array} = \begin{array}{|c|c|c|c|c|c|c|}\hline m_0 & 0 & 0 & 0 & 0 & 0 & 0 \\ m_1 & 0 & 0 & 0 & 0 & 0 & 0 \\ c_0 & 0 & 0 & 0 & 0 & 0 & 0 \\ c_1 & 0 & 0 & 0 & 0 & 0 & 0 \\ u_0 & 0 & 0 & 0 & 0 & 0 & 0 \\ u_1 & 0 & 0 & 0 & 0 & 0 & 0 \\ y_{00} & y_{01} & y_{02} & y_{03} & y_{04} & y_{05} & y_{06} \\ y_{10} & y_{11} & y_{12} & y_{13} & y_{14} & y_{15} & y_{16} \\ \hline m_2 & 0 & 0 & 0 & 0 & 0 & 0 \\ c_2 & 0 & 0 & 0 & 0 & 0 & 0 \\ u_2 & 0 & 0 & 0 & 0 & 0 & 0 \\ y_{20} & y_{21} & y_{22} & y_{23} & y_{24} & y_{25} & y_{26} \\ \hline m_3 & 0 & 0 & 0 & 0 & 0 & 0 \\ c_3 & 0 & 0 & 0 & 0 & 0 & 0 \\ u_3 & 0 & 0 & 0 & 0 & 0 & 0 \\ y_{30} & y_{31} & y_{32} & y_{33} & y_{34} & y_{35} & y_{36} \\ \hline m_4 & 0 & 0 & 0 & 0 & 0 & 0 \\ c_4 & 0 & 0 & 0 & 0 & 0 & 0 \\ u_4 & 0 & 0 & 0 & 0 & 0 & 0 \\ y_{40} & y_{41} & y_{42} & y_{43} & y_{44} & y_{45} & y_{46} \\ \hline m_5 & 0 & 0 & 0 & 0 & 0 & 0 \\ c_5 & 0 & 0 & 0 & 0 & 0 & 0 \\ u_5 & 0 & 0 & 0 & 0 & 0 & 0 \\ y_{50} & y_{51} & y_{52} & y_{53} & y_{54} & y_{55} & y_{56} \\ \hline m_6 & 0 & 0 & 0 & 0 & 0 & 0 \\ c_6 & 0 & 0 & 0 & 0 & 0 & 0 \\ u_6 & 0 & 0 & 0 & 0 & 0 & 0 \\ y_{60} & y_{61} & y_{62} & y_{63} & y_{64} & y_{65} & y_{66} \\ \hline \end{array} \quad (36)$$

After these preliminaries regarding the initial conditions, we approximated through iterative calculation steps,

$$x_k = x_{k-1} + \sum_{T=1}^{6} \frac{\Delta t^T}{T!} \cdot x_{T,k-1} \qquad x_{S,k} = x_{S,k-1} + \sum_{T=1}^{6} \frac{\Delta t^T}{T!} \cdot x_{TS,k-1} \quad (37)$$

At each integration step (Δt) we operated with a number of 20 Taylor series, of which 6 for ($m_{0k}, m_{1k}, c_{0k}, c_{1k}, u_{0k}, u_{1k}$) and 14 for ($y_{00k}, y_{01k}, ..., y_{06k}$).

It can be observed that 8 elements (signals) included in Taylor series are from the state vector component (x) and the other 12 are from the matrix component (x_S), each one included in (M_{dpx}).

The truncation error at each integration step (Δt) is proportional to $\left(\frac{\Delta t^7}{7!}\right)$, for (m, c, u, y_{00}), as well as to $\left(\frac{\Delta t^6}{6!}\right)$, for (y_{10}).

4. Case studies

4.1. Preliminaries

a) *The radiological field spread* has been estimated by the following parameters:

By 0*p* axis:

$$t_{pf} = 10; \quad \mu_{Tp} = 4{,}1; \quad \lambda_{Tp} = 1{,}5; \quad T_{1p} = 0{,}975; \quad T_{2p} = 1{,}463$$

$$p_f = 5; \quad p_d = 0{,}3 \cdot p_f; \quad A_{pd} = 50; \quad K_{pd} = 10; \quad \mu_P = 4$$

$$\lambda_P = 1{,}1; \quad P_1 = 0{,}595; \quad P_2 = 0{,}655$$

By 0*q* axis:

$$t_{qf} = 12; \quad \mu_{Tq} = 4{,}3; \quad \lambda_{Tq} = 1{,}7; \quad T_{1q} = 1{,}033; \quad T_{2q} = 1{,}757$$

$$q_f = 8; \quad q_d = 0{,}3 \cdot q_f; \quad A_{qd} = 45; \quad K_{qd} = 12; \quad \mu_Q = 4{,}2$$

$$\lambda_Q = 1{,}4; \quad Q_1 = 0{,}794; \quad Q_2 = 1{,}111$$

By 0*r* axis:

$$t_{rf} = 15; \quad \mu_{TR} = 4{,}5; \quad \lambda_{TR} = 1{,}9; \quad T_{1r} = 1{,}149; \quad T_{2r} = 2{,}184$$

$$r_f = 50; \quad r_d = 0{,}3 \cdot r_f; \quad A_{rd} = 55; \quad K_{rd} = 15; \quad \mu_R = 4{,}5$$

$$\lambda_R = 1{,}5; \quad R_1 = 4{,}444; \quad R_2 = 6{,}666$$

According to (24, 25), it resulted:

$$\mu_\tau = 4{,}321; \ \lambda_\tau = 1{,}711; \ T_1 = 1{,}85 \text{ and } T_2 = 3{,}16.$$

According to (11, 12), it resulted:

$$\mu_S = 4.416; \lambda_S = 1{,}445; \ S_1 = 4{,}71; S_2 = 6{,}81.$$

b) *The structure parameters*, and the equation coefficients of the system (29, 30) were:

$$K_M = 1;\ T_M = 0{,}055;\ K_E = K_r = 1;\ T_E = T_r = 0{,}06;\ T_R = 0{,}05$$

$$K_{PR} = \frac{T_1 + T_2}{2 \cdot K_{Ex} \cdot T_\Sigma};\quad K_{TR} = \frac{1}{2 \cdot K_{Ex} \cdot T_\Sigma};\quad K_{DR} = \frac{T_1 \cdot T_2}{2 \cdot K_{Ex} \cdot T_\Sigma} \qquad (38)$$

$$T_\Sigma = T_R + T_E + T_M$$

By convenient choice of (K_{Ex}), a flexible controller PID for relation (29) shown in Tables 2 and 3 has been ensured.

The intensity field X-ray reference signal (w_0) and the perturbation signal ($\tilde{u}_0$) in figure 5, present a continuous component on top of which periodic components may overlap.

c) The a*nalogical model for the spread of the radiological field* expressed by the second order partial differential equation in (31) presents the coefficients:

$$a_{00} = 1;\ a_{10} = T_1 + T_2 = 5{,}012;\ a_{20} = T_1 \cdot T_2 = 5{,}848;$$

$$a_{01} = S_1 + S_2 = 11;$$

$$a_{02} = S_1 \cdot S_2 = 32{,}08;\ a_{11} = (T_1 + T_2) \cdot (S_1 + S_2) = 57{,}75.$$

The proportionality coefficient $K_y = 1$, may be altered over large limits, since the variables presented in figures 1b, 1c, 1d, 2, 3 and 4, are asymptotic or non-asymptotic between 0 and 1.

4.2. Case study 1: System behavior in open loop

The control system in figure 5 may be considered in stopped reaction, respectively, $m_0 = 0$.

The R controller and the radiological field generator ensure a unitary transfer with a negligible delay of the reference signal $w_0 \cong a_0 \cong c_0 \cong u_0$.

The radiological field E generated by the control signal (u_0) develops inside a propagation space an intensity $y_{00}[t, s, u_{S0}(t)]$, representing the solution of partial differential equation (31).

Table 1 presents the evolution of the intensity of the above radiological field (y_{00}), with respect to time (t), with $w_0 = 10$, for 11 points from a Cartesian space, respectively (0,0,0),…(p_f, q_f, r_f).

Table 1. Intensities of the simulated radiological field in open loop

p	*q*	*r*	$t = 10^{-2}$	1	3	5	7	9	12	15	18	22
0	0	0	10^{-6}	0,65	3.47	5.98	7.68	8.71	9.48	9.79	9.90	9.965
$0.1 \cdot p_f$	$0.1 \cdot q_f$	$0.1 \cdot r_f$	10^{-6}	0.51	2.68	4.64	5.95	6.75	7.34	7.59	7.68	7.73
$0.2 \cdot p_f$	$0.2 \cdot q_f$	$0.2 \cdot r_f$	10^{-5}	0.43	2.29	3.96	5.08	5.76	6.27	6.48	6.56	6.60
$0.3 \cdot p_f$	$0.3 \cdot q_f$	$0.3 \cdot r_f$	10^{-4}	1.63	8.64	14.9	19.14	21.7	23.6	24.4	24.7	24.84
$0.4 \cdot p_f$	$0.4 \cdot q_f$	$0.4 \cdot r_f$	$5 \cdot 10^{-6}$	0.123	0.653	1.127	1.44	1.64	1.78	1.845	1.87	1.88
$0.5 \cdot p_f$	$0.5 \cdot q_f$	$0.5 \cdot r_f$	10^{-7}	0.044	0.233	0.403	0.517	0.586	0.638	0.660	0.667	0.671
$0.6 \cdot p_f$	$0.6 \cdot q_f$	$0.6 \cdot r_f$	$4 \cdot 10^{-8}$	0.022	0.115	0.198	0.255	0.289	0.315	0.325	0.329	0.331
$0.7 \cdot p_f$	$0.7 \cdot q_f$	$0.7 \cdot r_f$	$2 \cdot 10^{-8}$	0.010	0.056	0.097	0.124	0.141	0.153	0.159	0.160	0.161
$0.8 \cdot p_f$	$0.8 \cdot q_f$	$0.8 \cdot r_f$	10^{-8}	0.005	0.027	0.047	0.06	0.068	0.074	0.076	0.077	0.078
$0.9 \cdot p_f$	$0.9 \cdot q_f$	$0.9 \cdot r_f$	$5 \cdot 10^{-9}$	0.002	0.013	0.022	0.029	0.032	0.035	0.036	0.037	0.037
p_f	q_f	r_f	$2 \cdot 10^{-9}$	$1 \cdot 10^{-3}$	$6 \cdot 10^{-3}$	$1 \cdot 10^{-2}$	0.013	0.015	0.017	0.0176	0.0178	0.186

$$K_M = 0; K_v = 1; w_A = 10; K_{PR} = 1; K_{IR} = 0; K_{DR} = 0; K_{EX} = 15; t_f = 22$$

It may be observed that in the near vicinity of the radiation source application point, (0,0,0), the radiological field intensity (y_{00}) has a maximum value, presenting an exponential evolution which tends asymptotically towards the references value $w_0 = 10$. The further away we move from the source, towards the final penetration depth (p_f, q_f, r_f), the more the radiological field intensity (y_{00}) decreases.

The $(0{,}3 \cdot p_f; 0{,}3 \cdot q_f; 0{,}3 \cdot r_f)$ point corresponds to a structure perturbation (p_d, q_d, r_d), for which the intensity (y_{00}) presents a remarkable discontinuity, in conformity with figure 2, relation (16) and figure 4. It may arbitrarily be considered that this discontinuity presents a "*zoom effect*", by concentrating radiological field intensity (y_{00}). Of course the opposite may also be considered, if in (24) the amplitude $A_{vd} < 0$.

4.3. Case study 2: System behavior in control loop

In this case, the transducer M of radiological field intensity (y_{00}) achieves a control error $a = w - m$, using the measured signal (m) and a reference signal (w), which is processed by the R controller, with PID structure. Through the transfer function of the regulator,

$$\frac{Lc}{La} = \frac{K_{PR} + \frac{1}{s}K_{IR} + sK_{DR}}{1 + T_R \cdot s} \tag{39}$$

the three effects: proportional K_{PR}, integration K_{IR} and derivative K_{DR}, can be modified over large limits if the K_{EX} coefficient is wisely chosen from (38).

Table 2 presents the evolution of the radiological field intensity (y_{00}), with respect to time (t), with $w = 5$, for the same 11 points of the Cartesian space. By convenient adjustment of the controller R, an intensity $y_{00} \cong 5$ was ensured in steady state regime.

For $K_M = 1$; $K_v = 1$; $w = 5$; $t_f = 22$; K_{EX} conveniently chosen to ensure $y_{00} \cong 5$ in steady state regime, the evolution is non-periodically ascending towards $y_{00} \cong 5$, at $t_f \cong 22$. The values of curves are identical, which means that the numerical simulation stages have been performed correctly.

The only exception corresponds to the perturbation point $(0{,}3\,p_f$, $0{,}3q_f$, $0{,}3r_f)$, where the "*zoom effect*" of (y_{00}) presents a slight peak, at 6.45, then returning to the same asymptote $y_{00} \cong 5$.

In this perturbation regime, the relatively small value of $K_{EX} = 0{,}282$ constrained an important growth of the PID controller effects.

Table 2. Intensities of the simulated radiological field in control loop

p	q	r	y_{00}	K_{EX}	t=10^{-2}	1	3	5	7	9	12	15	18	22
0	0	0	y_{00A}	15	$6{\cdot}10^{-7}$	0.33	1.76	3.03	3.88	4.38	4.76	4.91	4.97	4.999
0.1 p_f	0.1 q_f	0.1 r_f	y_{00B}	11.6	$6{\cdot}10^{-7}$	0.33	1.76	3.03	3.88	4.39	4.76	4.91	4.97	4.999
0.2 p_f	0.2 q_f	0.2 r_f	y_{00C}	11.4	$1{\cdot}10^{-5}$	0.33	1.756	3.02	3.87	4.39	4.77	4.92	4.98	5.002
0.3 p_f	0.3 q_f	0.3 r_f	y_{00D}	0.282	$2{\cdot}10^{-4}$	2.28	5.62	6.45	6.33	5.99	5.54	5.27	5.13	5.05
0.4 p_f	0.4 q_f	0.4 r_f	y_{00E}	2.25	$5{\cdot}10^{-6}$	0.33	1.758	3.03	3.88	4.38	4.76	4.91	4.97	4.998
0.5 p_f	0.5 q_f	0.5 r_f	y_{00F}	1.01	$6{\cdot}10^{-7}$	0.33	1.76	3.03	3.88	4.38	4.76	4.91	4.97	4.997
0.6 p_f	0.6 q_f	0.6 r_f	y_{00G}	0.500	$6{\cdot}10^{-7}$	0.33	1.757	3.02	3.87	4.38	4.76	4.91	4.97	4.996
0.7 p_f	0.7 q_f	0.7 r_f	y_{00H}	0.245	$6{\cdot}10^{-7}$	0.33	1.751	3.02	3.87	4.37	4.76	4.91	4.97	4.999
0.8 p_f	0.8 q_f	0.8 r_f	y_{00I}	0.117	$6{\cdot}10^{-7}$	0.33	1.765	3.03	3.88	4.39	4.77	4.92	4.97	4.999
0.9 p_f	0.9 q_f	0.9 r_f	y_{00J}	0.057	$6{\cdot}10^{-7}$	0.33	1.75	3.01	3.86	4.37	4.75	4.90	4.97	4.994
p_f	q_f	r_f	y_{00K}	0.027	$6{\cdot}10^{-7}$	0.33	1.76	3.03	3.88	4.39	4.76	4.92	4.97	4.998

Thus, a constant value of field intensity at $y_{00}(t_f) \cong 5$ in steady state regime, for reference $w = 5$, over all 11 points y_{00A}, y_{00B},…, y_{00K} has been ensured.

Table 3. Influence of the K_{EX} coefficient on the R controller

y_{00}	K_{EX}	K_{PR}	K_{IR}	K_{DR}	$y_{00}(t_f)$	$u_S(t_f)$
y_{00A}	15	1.0125	0.202	1.181	4.999	5.009
y_{00B}	11.6	1.309	0.261	1.527	4.999	6.464
y_{00C}	11.4	1.332	0.266	1.554	5.002	10.68
y_{00D}	0.282	53.86	10.74	62.84	5.05	19.69
y_{00E}	2.25	6.750	1.345	7.876	4.998	37.51
y_{00F}	1.01	15.037	3.00	17.546	4.997	74.45
y_{00G}	0.500	30.37	6.06	35.44	4.996	150.71
y_{00H}	0.245	62	12.37	72.33	4.995	308.94
y_{00I}	0.117	129.8	25.9	151.46	4.999	639.7
y_{00J}	0.057	266.4	53.16	310.9	4.994	1329.8
y_{00K}	0.027	562.5	112.2	656.35	4.998	2781

The further the M transducer is placed from the radiological field-generating device, the more intense the three effects of the controller, resulting in larger K_{PR}, K_{IR} *and* K_{DR} coefficients.

Near the structural discontinuity, corresponding to the y_{00D} concentration, the controller ensures the attenuation of the resulting perturbation, by constraining larger values for the three PID effects.

In a stationary regime $y_{00}(t_f) \cong 5$, the execution signals $u_S(t_f)$ present roughly uniform increasing values, for progressively increasing distance of the transducer M from the field generating device.

Conclusions

The paper studies a modeling approach of a radiological propagation process, based on a system of three differential equations and a partial derivative equation (PDE) with three space variables and one time variable.

For analogical modeling it operates using *the matrix of partial derivatives for the state vector* M_{dpx}, associated with Taylor series for computational simulation.

A controller (R) can be tuned in order to ensure the control of radiological field intensity at different points where field sensors and transducers are located.

Multiple degrees of freedom can be ensured using structural parameters of the model and external elements such as the above mentioned controller, transducers and sensors. Altering of environmental propagation can be distinguished using structural parameters $(\mu_{...})$ and $(\lambda_{...})$, in time as well as in space.

The model accounts for the presence of structural tissue discontinuity. Specific time-space dynamics are taken into account for each space axis (O_p, O_q, O_r).

Units of measurement for length (p,q,r), time (t), execution signals (u), radiation intensity (y) and other parameters may be chosen as needed, but will only be valid for each individual case study.

The PDE model may be adapted for various processes of radiation or thermal propagation, with applications in both medical diagnosis and treatment.

R E F E R E N C E S

[1] N.M. Roman, M.S. Munteanu, *Măsurarea, modelarea şi simularea proceselor biomedicale*, (Mediamira, Cluj-Napoca, Romania 2002), ISBN 973-9357-02-04.

[2] H.A. Colosi, E.H. Dulf, M.N. Roman, A. Achimaş, *Modeling and Simulation of Controlled Orthodontic Tipping and Translation of Single-rooted Teeth*, IEEE International Conference on Automation, Quality and Testing, Robotics, IEEE Catalog Number:CFP08AQT-CDR, ISBN:978-1-4244-2577-8 (2008).

[3] N.M. Roman, H.Colosi, M.Pusca, *Digital Simulation for Computer Control of Radiological Devices: A Preliminary Model Using Partial Differential Equations*, MediTech 2009, Cluj-Napoca, Romania, Springer, ISBN 978-3-642-04291-1, pp. 37-42 (2009).

[4] N.M. Roman, V. Dan, R.V. Ciupa, V. Pompas, *Hyperthermia Control Using a Computer Microwave System in Cancer Therapy*, IFMBE Proceedings **25**/VI, p. 103, München (2009).

[5] G. Sajin, M. Sajin, G. Gavriloaia, *Aplicaţii biologice ale radiaţiilor electro-magnetice*, (Ed. Academiei Tehnice Militare, Bucureşti, Romania, 2003), ISBN 973-640-010-7.

[6] C.X. Yu, C.J. Amies, M. Svatos, *Planning and delivery of intensity-modulated radiation therapy*, Med. Phys. **35**,5233 (2008).

[7] T. Colosi, M.I. Abrudean, E.H. Dulf, M.L. Ungureşan, *Numerical Modeling and Simulation Method for Lumped and Distributed Parameters Processes, with Taylor Series and Local Iterative Linearization*, (Ed. Mediamira, Cluj-Napoca, Romania, 2008), ISBN 978-973-713-207-9.

[8] T. Colosi, M.L. Ungureşan, E.H. Dulf, R.C. Cordoş, *Introduction to Anlogical Modeling and Numerical Simulation, with (M_{pdx}) and Taylor Series for Distributed Parameters Processes*, (Ed. Galaxia Gutenberg, Târgu-Lăpuş, Romania 2009), ISBN 978-973-141-192-7.